

Dirac Line Nodes in Inversion Symmetric Crystals

Youngkuk Kim,¹ Benjamin J. Wieder,² C. L. Kane,² and Andrew M. Rappe¹

¹*The Makineni Theoretical Laboratories, Department of Chemistry,
University of Pennsylvania, Philadelphia, Pennsylvania 19104-6323, USA*

²*Department of Physics and Astronomy, University of Pennsylvania, Philadelphia, Pennsylvania 19104-6396, USA*
(Dated: April 22, 2015)

We propose and characterize a new \mathbb{Z}_2 class of topological semimetals with a vanishing spin-orbit interaction. The proposed topological semimetals are characterized by the presence of bulk one-dimensional (1D) Dirac Line Nodes (DLNs) and two-dimensional (2D) nearly-flat surface states, protected by inversion and time-reversal symmetries. We develop the \mathbb{Z}_2 invariants dictating the presence of DLNs based on parity eigenvalues at the parity-invariant points in reciprocal space. Moreover, using first-principles calculations, we predict DLNs to occur in Cu_3N near the Fermi energy by doping non-magnetic transition metal atoms, such as Zn and Pd, with the 2D surface states emerging in the projected interior of the DLNs. This paper includes a brief discussion of the effects of spin-orbit interactions and symmetry-breaking as well as comments on experimental implications.

A recent development in condensed matter physics has been the discovery of semimetallic features in electronic band structures protected by the interplay of symmetry and topology. A tremendous amount of progress has been made in materials with strong spin-orbit interactions, such as the surface states of topological insulators [1, 2] and topological crystalline insulators [3], as well as the gapless bulk states of Weyl and Dirac semimetals [4–6]. Related topological phenomena can occur in materials with vanishing (or weak) spin-orbit interactions [7]. Indeed, the prototypical topological semimetal is graphene [8], which exhibits Dirac points that are robust to the extent that the spin-orbit interaction in carbon is weak. In the absence of spin-orbit interactions, the Dirac points in graphene are topologically protected by the combination of inversion and time-reversal symmetries.

In this paper we study a related phenomenon for three dimensional (3D) materials with weak spin-orbit interaction. We show that the combination of inversion and time-reversal symmetries protects Dirac line nodes (DLNs), for which the conduction band and valence band meet along a line in momentum space, and we predict realistic materials in which they should occur. DLNs have been discussed previously in the context of models that have an additional chiral symmetry, which can arise on a bipartite lattice with only nearest neighbor hopping. In this case, the DLN can be constrained to occur at zero energy. However, chiral symmetry is never expected to be an exact symmetry of a band structure. We will show that despite the absence of chiral symmetry, the line node is protected, though it is not constrained to sit at a constant energy. We will show, however, that in the vicinity of a band inversion transition, a DLN can occur in the form of a small circle, whose energy is approximately flat. The presence of such a Dirac circle has interesting consequences for the surface states, and we show that on the projected interior of the Dirac circle, the surface exhibits a nearly flat band, which must be half-filled when

the surface is electrically neutral. Such surface states could be an interesting platform for strong correlation physics. We introduce a class of materials and use first-principles density functional theory (DFT) calculations to show that they can be tuned through the band inversion transition and exhibit the predicted Dirac circle, as well as a more complex nodal structure. A similar DLN near an inversion transition has recently been predicted in a 3D graphene network [9, 10]. Recently, DLNs also have been proposed in systems with strong spin-orbit interactions, such as perovskite irridates [11, 12] and non-centrosymmetric semimetals [13], but in those systems the mechanism of symmetry protection is different.

We will begin by elucidating the topological constraints that inversion and time-reversal symmetries impose. We will then introduce a \mathbb{Z}_2 topological invariant (related to the invariant characterizing a 3D topological insulator) which signifies the presence of DLNs. We will then present DFT calculations on transition metal-doped Cu_3N that predict a Dirac circle, as well as nearly-flat boundary modes. We will then introduce a simple low-energy $\mathbf{k} \cdot \mathbf{p}$ model that explains the appearance of the Dirac circle at a band inversion, and allows for a simple description of the resulting boundary modes.

Consider a 3D Bloch Hamiltonian $\mathcal{H}(\mathbf{k})$ that is invariant under inversion \mathcal{P} and time-reversal \mathcal{T} . In the absence of spin-orbit interactions we may consider $\mathcal{T}^2 = +1$. The occupied Bloch eigenstates are characterized by a Berry connection $\mathbf{A}(\mathbf{k}) = -i \sum_n \langle u_n(\mathbf{k}) | \nabla_{\mathbf{k}} u_n(\mathbf{k}) \rangle$. \mathcal{P} and \mathcal{T} symmetries constrain the Berry phase, $\omega(C) = \exp i \oint_C \mathbf{A} \cdot d\mathbf{k}$, on any closed loop C in momentum space, to satisfy $\omega(C) = \omega(-C)$ and $\omega(C) = \omega(-C)^*$, respectively. It follows that loops C are characterized by a \mathbb{Z}_2 topological invariant $\omega(C) = \pm 1$ [14]. The non-trivial loops $\omega(C) = -1$ must enclose a degeneracy. In two dimensions, this explains the symmetry protection of the Dirac points in graphene. In three dimensions, it guarantees that a line of degeneracies must pierce any surface

bounded by C .

The parity eigenvalues $\xi_n(\Gamma_a) = \pm 1$ of the occupied Bloch states at the 8 parity-invariant momenta Γ_a provide an important constraint that allows us to identify topologically protected line nodes. First, consider a time-reversal invariant loop $C_{ab} = c_{ab} - \bar{c}_{ab}$ that connects Γ_a and Γ_b along two time-reversed paths c_{ab} and \bar{c}_{ab} . In the supplementary material we prove that the Berry phase on this loop satisfies

$$\omega(C_{ab}) = \xi_a \xi_b; \quad \xi_a = \prod_n \xi_n(\Gamma_a). \quad (1)$$

If we now consider four parity-invariant points, the contour $C_{ab} - C_{cd}$ defines the boundary ∂S_{abcd} of a surface S_{abcd} in momentum space. The Berry phase on ∂S_{abcd} counts the number of DLNs $N(S_{abcd})$ that pierce that surface. We thus conclude that

$$(-1)^{N(S_{abcd})} = \xi_a \xi_b \xi_c \xi_d. \quad (2)$$

Thus, when $\xi_a \xi_b \xi_c \xi_d = -1$ there must be an odd number of DLN piercing any surface S_{abcd} , with the simplest case being just a single one. This relation is quite similar to the topological invariants $(\nu_0; \nu_1 \nu_2 \nu_3)$ characterizing a (strong or weak) \mathbb{Z}_2 topological insulator in the presence of spin-orbit interactions [15, 16]. Indeed, in a topological insulator with $\xi_a \xi_b \xi_c \xi_d = -1$, when the spin-orbit interaction is turned off a DLN must appear, because the system can not be adiabatically connected to a trivial insulator.

This connection to the parity eigenvalues suggests a route towards realizing the DLNs: Starting with a trivial insulator, invert a pair of opposite-parity bands. At the inversion transition a small Dirac circle will necessarily emerge and grow. In the following we will predict a class of real materials which exhibits this behavior, and analyze the low-energy structures which emerge.

Searching for materials that consist of light elements and preserve \mathcal{T} and \mathcal{P} symmetries, we find that copper nitride, Cu_3N , a narrow-gap semiconductor ($E_g \sim 0.3$ eV) [17], fosters DLNs near the Fermi level via an insulator-to-metal transition driven by doping transition metal atoms. Copper nitride, first synthesized in 1937 [17], is stable in air at room temperature with a cubic anti- ReO_3 structure in space group 221 ($\text{Pm}\bar{3}\text{m}$). It contains a rather large void at the center of the cubic unit cell, as shown in Fig. 1. This void can host extrinsic atoms such as N [18], Li [19, 20], Pd [21–25], Rh, Ru [25], Zn, Ni, Cd [21], Cu [20, 26], Fe, Ti [27], Ag [28], La, Ce [29], as well as many other transition-metal atoms [30]. In particular Ni, Cu, Pd, An, Ag, and Cd [21] are found to drive an electronic transition in Cu_3N into a semimetal without breaking \mathcal{T} symmetry [30], by which we expect that DLNs form near the Fermi energy.

To demonstrate the existence of DLNs in the transition metal-doped Cu_3N , we perform first-principles cal-

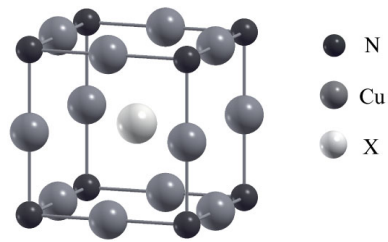


FIG. 1. Crystal structure of Cu_3NX . X represents a transition metal atom intercalated at the body-center of the cubic unit cell of Cu_3N in an anti- ReO_3 structure.

culations based on DFT. We employ the Perdew–Burke–Ernzerhof-type generalized gradient approximation [31] as implemented in the QUANTUM ESPRESSO package [32]. Norm-conserving, optimized, designed nonlocal pseudopotentials are generated by the OPIUM package [33, 34]. The wave functions are expanded in a plane-wave basis with an energy cutoff of 680 eV. We initially consider the spin-orbit interaction based on a scalar-relativistic pseudopotential [35], and later, we will discuss the effect of spin-orbit interactions, based on a fully-relativistic non-collinear scheme.

The low-energy electronic structures of Cu_3NX are more or less similar for $X = \{\text{Ni}, \text{Cu}, \text{Pd}, \text{An}, \text{Ag}, \text{Cd}\}$, as reported in Ref. [21]. Here we present the results of Cu_3NZn and Cu_3NPd as representatives of transition metal-doped Cu_3N systems. Note that these are extreme cases where the transition metal atoms are maximally doped [36]. In Cu_3NZn the conduction and valence bands are mainly comprised of conduction A_{2u} and valence A_{1g} states near the Fermi energy. As shown in Fig. 2, these bands are inverted at the X points, forming two-dimensional (2D) Dirac points on the X – M and R – X lines (enclosed by red circles in the figure). These Dirac points signal the presence of a DLN enclosing X . Although there are more degenerate points near the Fermi level, and bands crossing the Fermi energy near the R point, we will simplify and here focus only on the bands near X . On the other hand, the conduction and valence bands of Cu_3NPd are comprised of T_{2g} and T_{1u} states, which are inverted at the R point, forming the Dirac points on the R – X and M – R lines. These Dirac points are in fact parts of a DLN that encloses the R point, as shown below.

The nodal lines of the conduction and valence bands in the 3D BZ are shown in Fig. 3. As mentioned above, DLNs appear near the X points in the Cu_3NZn system. The cubic symmetry of the system dictates three DLNs encircling the three inequivalent X points $X^r = \pi\hat{r}/a$, where $r = x, y$, and z . Similarly, Cu_3NPd also exhibits three DLNs due to the cubic symmetry, but since they appear enclosing the R point, they form in a gyroscope shape. In both systems, the DLNs are contained in three mirror-invariant planes at X^x , X^y , and X^z , due to the

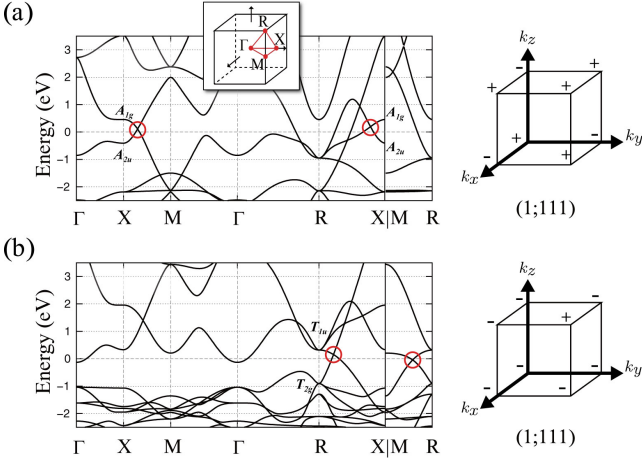


FIG. 2. (color online) Electronic structures and \mathbb{Z}_2 indices of (a) Cu_3NZn and (b) Cu_3NPd . Bands are drawn along the high-symmetry lines of the BZ (inset). The Dirac points are indicated by red circles. Parity eigenvalues are illustrated at the eight parity-invariant points in the first octant of the BZ.

corresponding mirror symmetries. We expect that breaking the mirror symmetries should unlock the DLNs from the mirror planes, but that the DLNs will survive as they are protected by \mathcal{P} and \mathcal{T} .

The appearance of DLNs agrees with the topological prediction of \mathbb{Z}_2 invariants $(\nu_0; \nu_1\nu_2\nu_3)$, calculated from the parity analysis. In Cu_3NZn , parities at the eight time-reversal invariant momenta $(\Gamma, 3X, 3M, R)$ give $(\nu_0; \nu_1\nu_2\nu_3) = (1; 111)$, which dictates that there should be DLNs threading half the invariant plane at $X^r = \pi\hat{r}/a$ ($r = x, y, z$) an odd number of times. The three DLNs enclosing the X points fulfill this topological constraint (see the supplementary material for more details of this analysis). Similarly, in Cu_3NPd we find that $(\nu_0; \nu_1\nu_2\nu_3) = (1; 111)$, which is also in accordance with the formation of the three DLNs enclosing R . In this case, each invariant plane at X^r is threaded three times by all three DLNs.

A low-energy $\mathbf{k} \cdot \mathbf{p}$ Hamiltonian describing the conduction A_{2u} and valence A_{1g} states, which form the DLNs in Cu_3NZn , captures the essential features of the DLNs. Near X^r , symmetries dictate a two-band Hamiltonian

$$\mathcal{H}_r = (\bar{\epsilon} + a_\perp |\mathbf{q}_\perp|^2 + a_r q_r^2) \mathbb{I}_r + v q_r \tau^y + (\Delta\epsilon + b_\perp |\mathbf{q}_\perp|^2 + b_r q_r^2) \tau^z, \quad (3)$$

where $\mathbf{q} = \mathbf{k} - X^r$, \perp represents the normal components to \hat{r} , and the Pauli matrices $\{\mathbb{I}_r, \tau^i\}$ describe the A_{1g} and A_{2u} states. The form of \mathcal{H}_r is uniquely determined by inversion $\mathcal{P} = \tau^z$ and time-reversal $\mathcal{T} = K$ (K being complex conjugation), together with the D_{4h} point group symmetries of X . It gives energy eigenvalues

$$E_\pm(\mathbf{q}) = \bar{\epsilon} + a_\perp |\mathbf{q}_\perp|^2 + a_r q_r^2 \pm \sqrt{(\Delta\epsilon + b_\perp |\mathbf{q}_\perp|^2 + b_r q_r^2)^2 + v^2 q_r^2}. \quad (4)$$

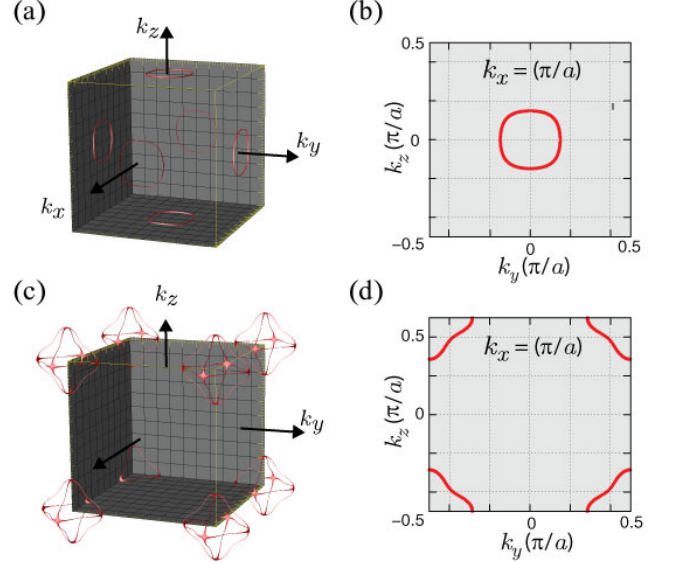


FIG. 3. (color online) Dirac line nodes in the Brillouin Zone (BZ). (a) and (b) Cu_3NZn , and (c) and (d) Cu_3NPd . The DLNs are illustrated by red curves in the 3D BZ [(a) and (c)] and on the 2D boundary plane of the BZ at $k = X^x$ [(b) and (d)].

A DLN forms at $q_r = 0$ and $|\mathbf{q}_\perp|^2 \equiv q_0^2 = -\Delta/b_\perp$, when the bands are inverted ($\Delta\epsilon < 0$). The DFT results determine $\Delta\epsilon \sim -0.4$ eV. In Cu_3NPd , unlike in Cu_3NZn , there are conduction T_{2g} and valence T_{1u} states, instead leading to a six-band Hamiltonian \mathcal{H} . However, this can be decomposed into three copies of \mathcal{H}_r with $r = x, y$, and z and $\mathcal{H} = \mathcal{H}_x \oplus \mathcal{H}_y \oplus \mathcal{H}_z$, giving rise to three gyroscope-shaped DLNs. Therefore, the essential features of the DLNs should be the same between Cu_3NZn and Cu_3NPd , aside from the former having a single DLN occurring in three inequivalent valleys of the BZ (X points) and the latter having three DLNs in a single valley (R point).

This model Hamiltonian also describes boundary modes. Consider a boundary perpendicular to \hat{r} in which $\Delta\epsilon$ varies between a negative (inverted) value and a large positive value. Fixing q_\perp and considering the theory to linear order in $q_r \rightarrow -i\partial_r$,

$$\mathcal{H}_z(\mathbf{q}) = -iv\tau^y\partial_r + (\Delta\epsilon(r) + b_\perp q_\perp^2)\tau^z + (\bar{\epsilon} + a_\perp q_\perp^2)\mathbb{I}_r. \quad (5)$$

For each k_\perp this defines a Jackiw-Rebbi problem [37]. When $\Delta\epsilon + b_\perp k_\perp^2 < 0$ there will be a boundary mode at the surface. In general the boundary band is not flat, but disperses for $k_\perp < k_F$

$$\epsilon_0(k_\perp) = \bar{\epsilon} + a_\perp k_\perp^2 \leq 0. \quad (6)$$

If $a = 0$ however, the surface band is flat. This reflects an additional chiral symmetry $\{\mathcal{H}, \tau^x\} = 0$ at this point. In this model, the value of a is related to the difference of the effective masses of the A_{1g} and A_{2u} bands. If the surface in the absence of inversion is electrically neutral,

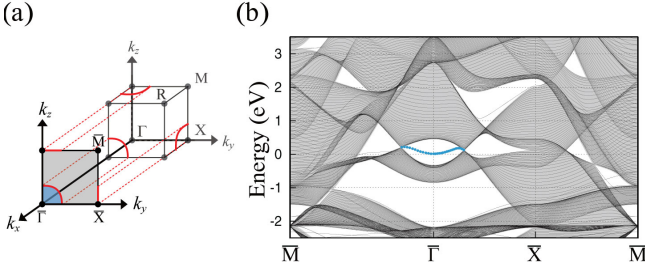


FIG. 4. (color online) Two-dimensional surface electronic structure for Cu_3NZn . (a) First octant of three-dimensional Brillouin zone (BZ) of Cu_3NZn projected onto the two-dimensional surface BZ of the (100) surface and (b) surface electronic band structure. The Dirac line nodes (DLNs) and the projected interior of DLNs are illustrated with the red and blue schemes, respectively. The slab bands are shown in black lines and surface states in the enclosed region are shown in blue lines. The shaded region represents bulk bands projected onto the BZ of the (100) surface along k_x .

then after inversion the surface will be neutral when the surface band is *half-filled*. This leads to a narrow surface band, where electron density $q_0^2/4\pi = |\Delta\epsilon|/4\pi b_\perp$ is controlled by the degree of band inversion. In the absence of screening from other bands, this surface band will tend to be pinned at the Fermi energy.

To study the surface states in Cu_3NZn , we calculate the band structures of a slab geometry with 40 unit cells, exposing the (100) Cu_2N surfaces to vacuum. Our calculation from first principles predicts that nearly-flat surface states emerge in the interiors of projected DLNs connecting the Dirac nodes, as shown in Fig. 4. The slab band structure exhibits the weakly-dispersing surface states near $\bar{\Gamma}$ in the projected interior of the DLN. The topological surface states resulting from closed DLNs are half-filled and nearly flat, providing a unique venue for interesting strong-correlation and transport physics.

The strong spin-orbit interaction can induce diverse topological phases in DLN semimetals, including topological insulators, 3D Dirac semimetals [5, 38], or even other DLN semimetals [12]. Analogously to graphene, spin-orbit interaction can gap out DLNs and drive the system to a topologically-insulating phase. The resultant topological insulator should have the same topological \mathbb{Z}_2 indexes as the DLN semimetal from which it originated. More interestingly, an additional crystalline symmetry may protect a part of the DLN in a symmetry-invariant region of the BZ, resulting in topological Dirac semimetals or crystalline symmetry-protected DLNs with strong spin-orbit interactions. We have tested the effect of spin-orbit interaction in Cu_3NPd using a fully-relativistic non-collinear scheme, and indeed found that C_4 symmetry along the R - M line protects the Dirac point on the line, while the spin-orbit coupling otherwise opens a gap (with maximum size of ~ 62 meV on the R - X line), thus giving rise to a 3D Dirac semimetal phase in a strong

spin-orbit interacting regime. Note that Cu_3NPd is an extreme case where Pd is maximally doped, and thus the spin-orbit interactions due to Pd $4d$ states are maximized. The spin-orbit interaction can be controlled either by the Pd-doping concentration, or by doping other group-X transition-metal atoms, such as Ni, Pd, and Pt. We thus expect both the DLN semimetal and 3D Dirac semimetal phases should be accessible in the Cu_3N system.

In summary, we have demonstrated that the combination of inversion and time-reversal symmetries allows for the \mathbb{Z}_2 classification of topological semimetals under vanishing spin-orbit interactions. The proposed topological semimetals are characterized by the presence of bulk DLNs and nearly-flat surface states, protected by inversion and time-reversal symmetries. Our first-principles calculations predict that the proposed topological phase can be observed in Cu_3N by doping with a class of non-magnetic transition metal atoms X, where $X = \{\text{Ni}, \text{Cu}, \text{Pd}, \text{Ag}, \text{Cd}\}$. The 2D surface states predicted for the DLN semimetal can hopefully be experimentally observed through, for example, ARPES in Cu_3NX_x , using the doping concentration x as a knob to control the sizes of the closed DLN and the enclosed surface band. Doping with heavier atoms can also be used to potentially observe spin-orbit-induced topological phases.

While this manuscript was in the final stages of preparation we learned of recent work proposing DLN in Ca_3P_2 [39]. YK acknowledges support from NSF grant DMR-1120901. CLK acknowledges support from a Simons Investigator grant from the Simons Foundation. AMR acknowledges support from the DOE Office of Basic Energy Sciences, under grant number DE-FG02-07ER15920. Computational support is provided by the HPCMO of the U.S. DOD and the NERSC of the U.S. DOE.

SUPPLEMENTARY MATERIAL FOR DIRAC LINE NODES IN INVERSION SYMMETRIC CRYSTALS

Proof of Eqn. (1).

Here we prove that the path integral of a Berry connection $\mathbf{A}(\mathbf{k}) = -i \sum_n \langle u_n(\mathbf{k}) | \nabla_{\mathbf{k}} u_n(\mathbf{k}) \rangle$

$$\omega(C_{ab}) = e^{i \oint_{C_{ab}} \mathbf{A} \cdot d\mathbf{k}} \quad (\text{S1})$$

on a loop $C_{ab} = c_{ab} - \bar{c}_{ab}$ that connects two parity- and time-reversal-invariant points Γ_a and Γ_b along the two time-reversal paths c_{ab} and \bar{c}_{ab} (See Fig. S1) can be obtained by the parity eigenvalues $\xi_n(\Gamma_a) = \pm 1$ of the occupied Bloch states at parity-invariant momenta Γ_a

$$\omega(C_{ab}) = \xi_a \xi_b; \quad \xi_a = \prod_n \xi_n(\Gamma_a). \quad (\text{S2})$$

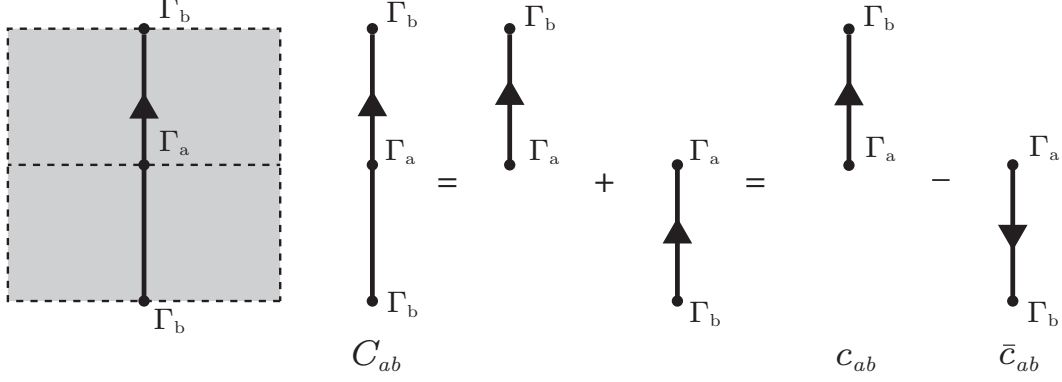


FIG. S1. Invariant loop C_{ab} in the Brillouin zone (BZ). The invariant loop $C_{ab} = c_{ab} - \bar{c}_{ab}$ connects two invariant points Γ_a and Γ_b , where \bar{c}_{ab} is a path from Γ_a to Γ_b along the time-reverse of c_{ab} .

It follows that

$$\begin{aligned} \omega(C_{ab}) &= e^{i(\int_a^b \mathbf{A}(\mathbf{k}) \cdot d\mathbf{k}|_{c_{ab}} - \int_a^b \mathbf{A}(\mathbf{k}) \cdot d\mathbf{k}|_{\bar{c}_{ab}})} \\ &= e^{i \int_a^b (\mathbf{A}(\mathbf{k}) - \mathbf{A}(-\mathbf{k})) \cdot d\mathbf{k}|_{c_{ab}}}. \end{aligned} \quad (\text{S3})$$

Inversion symmetry (\mathcal{P}) guarantees that $|u_n(-\mathbf{k})\rangle = e^{i\beta_n(\mathbf{k})} \mathcal{P}|u_n(\mathbf{k})\rangle$. It then follows that $\mathbf{A}(\mathbf{k}) - \mathbf{A}(-\mathbf{k}) = \nabla_{\mathbf{k}} \sum_n \beta_n(\mathbf{k})$, so that

$$\omega(C_{ab}) = e^{i \sum_n \beta_n(\Gamma_b) - \beta_n(\Gamma_a)}. \quad (\text{S4})$$

Now consider $P(\mathbf{k}) = \prod_n \langle u_n(-\mathbf{k}) | \mathcal{P} | u_n(\mathbf{k}) \rangle = e^{-i \sum_n \beta_n(\mathbf{k})}$. For a parity-invariant point Γ_i , $P(\Gamma_i) = \prod_n \xi_n(\Gamma_i)$, where $\xi_n(\Gamma_i) = \langle u_n(\Gamma_i) | \mathcal{P} | u_n(\Gamma_i) \rangle$ is the parity eigenvalue. We thus prove Eqn. (S2).

\mathcal{Z}_2 topological invariants and Dirac line nodes of Cu_3NZn

The topological invariant $\xi_a \xi_b \xi_c \xi_d = -1$ dictates that for any invariant surface S_{abcd} of the BZ, hosting four invariant momenta Γ_i ($i = a, b, c, d$), there will be an odd number of Dirac line nodes (DLNs) intersecting the half surface at \mathbf{k} (and the other half at $-\mathbf{k}$). Here we show that the DLNs that appear in Cu_3NZn satisfy this topological constraint. The cubic BZ of Cu_3NZn has eight distinct invariant momenta ($\Gamma, 3X, 3M, R$), and the parity eigenvalues at the high-symmetry momenta are calculated as $(\xi(\Gamma), \xi(X), \xi(M), \xi(R)) = (1, -1, 1, 1)$ as shown in Fig S2. Similar to the \mathcal{Z}_2 topological invariants of topological insulators [15], \mathcal{Z}_2 topological invariants $(\nu_0; \nu_1 \nu_2 \nu_3)$ can be defined in the DLN semimetals as

$$(-1)^{\nu_0} = \prod_{n_j=0,1} \xi_{n_1 n_2 n_3}, \quad (\text{S5})$$

$$(-1)^{\nu_{i=1,2,3}} = \prod_{n_j \neq i=0,1} \xi_{n_1 n_2 n_3}, \quad (\text{S6})$$

where $\xi_{i=(n_1 n_2 n_3)}$ are parity eigenvalues at the eight invariant momenta, $\Gamma_{i=(n_1 n_2 n_3)} = (n_1 \mathbf{b}_1 + n_2 \mathbf{b}_2 + n_3 \mathbf{b}_3)/2$, with $n_j = 0, 1$, and the primitive reciprocal lattice vectors \mathbf{b}_i . The \mathcal{Z}_2 invariants in Cu_3NZn are then obtained as $(\nu_0; \nu_1 \nu_2 \nu_3) = (1; 111)$, which dictate that an odd number of DLNs will pierce half the nontrivial invariant surfaces, S_{1467} , S_{2457} , and S_{3567} (See Fig. S2).

First-principles calculations show that three distinct DLNs appear in Cu_3NZn , contained in the boundary planes of the BZ as shown in Fig. S3. For convenience, we will refer to the DLN near the Γ_i as L_i , where $i = 1, 2, 3$. The DLNs in Cu_3NZn form in a manner that is consistent with the topological constraint, imposed by $(\nu_0; \nu_1 \nu_2 \nu_3) = (1; 111)$. To show this, we first consider an L_3 that encloses Γ_3 in the BZ. As shown in Fig. S3, L_3 intersects three invariant surfaces, referred to as S_{3567} , S_{0235} , and S_{0136} . The \mathcal{Z}_2 topological invariants $(\nu_0; \nu_1 \nu_2 \nu_3) = (1; 111)$ dictate that S_{3567} is nontrivial, and S_{0235} and S_{0136} are trivial, so that the nontrivial S_{3567} will be pierced by an odd number of DLNs, while the trivial S_{0136} and S_{0235} planes will be pierced by an even (including zero) number of DLNs. It is clear from Fig. S3 that the trivial S_{0235} and S_{0136} planes are pierced by two DLNs (L_3 and L_1 for S_{0136} , and L_3 and L_2 for S_{0235}), and is thus consistent with $\xi_a \xi_b \xi_c \xi_d = 1$, where $(abcd) = (0235), (0136)$. The nontrivial S_{3567} plane also satisfies the corresponding topological constraint. To show this, we construct a \mathcal{T} -invariant loop \tilde{C}_{35} that connects Γ_3 and Γ_5 avoiding the intersection with L_3 on the plane. The loop c_{35} connecting Γ_3 and Γ_5 is bent down in the $-k_z$ direction, while its time-reversed partner \bar{c}_{35} is bent up in the k_z direction, as shown in Fig. S4. From the figure, it is clear that the invariant surface S_{3567} , containing \tilde{C}_{35} is pierced once by L_3 in its half plane, thus satisfying the topological constraint imposed by $\xi_3 \xi_5 \xi_6 \xi_7 = -1$. Therefore, the appearance of L_3 satisfies the topological constraint. For the other inequivalent DLNs L_1 and L_2 , the cubic symmetry of Cu_3NZn allows

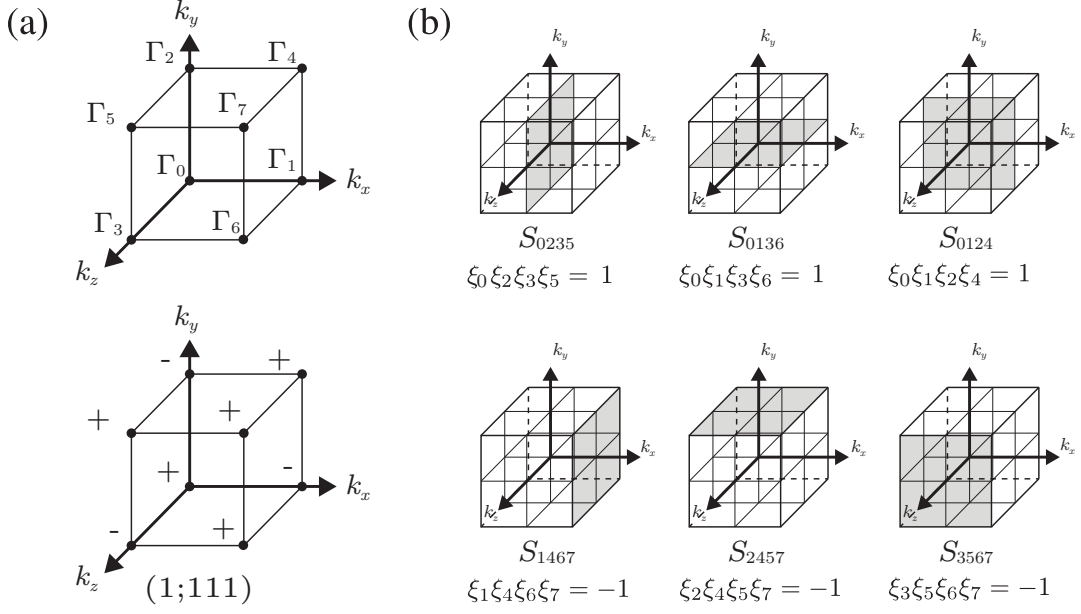


FIG. S2. Six invariant surfaces S_{abcd} in Cu_3NZn . (a) First octant of three-dimensional (3D) BZ. ξ_i of Cu_3NZn are presented at parity-invariant momenta Γ_i , which determine the $(\nu_0; \nu_1 \nu_2 \nu_3) = (1; 111)$ phase. (b) Shaded regions represent three trivial invariant planes (top panel) and three nontrivial invariant planes (bottom panel).

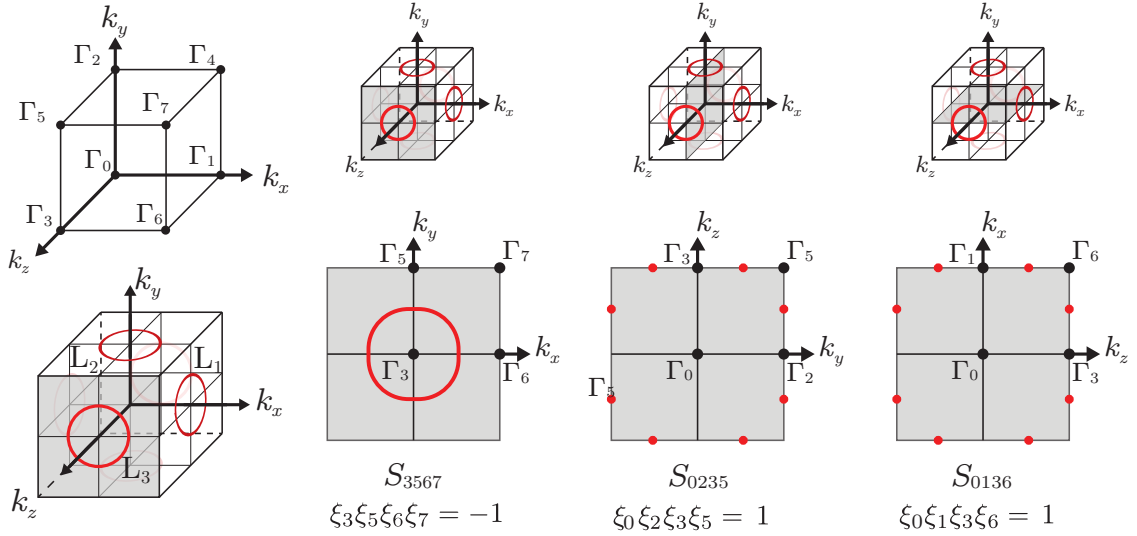


FIG. S3. Dirac line nodes (DLNs) and invariant planes in the BZ of Cu_3NZn . Red circles represent the DLNs. The grey-shaded planes illustrate the invariant planes that the DLN at Γ_3 point (L_3) intersects, one of which (S_{3567}) is nontrivial and the other two (S_{0235} and S_{0136}) are trivial. The intersecting position is depicted by red scheme on the planes.

us to apply the same argument for L_1 and L_2 to conclude that all the DLNs in Cu_3NZn obey the topological constraints characterized by \mathbb{Z}_2 topological invariants $(\nu_0; \nu_1 \nu_2 \nu_3) = (1; 111)$.

Band structures beyond Cu_3NZn and Cu_3NPd

In this section we extend our discussion of the material realization of DLN semimetals. We demonstrate that DLNs can occur in Cu_3N by doping a more general class of non-magnetic 3d and 4d transition metals (TMs) atoms in the X , XI , and XII groups of the periodic table, and that Cu_3NPd_x can realize DLNs in a low-

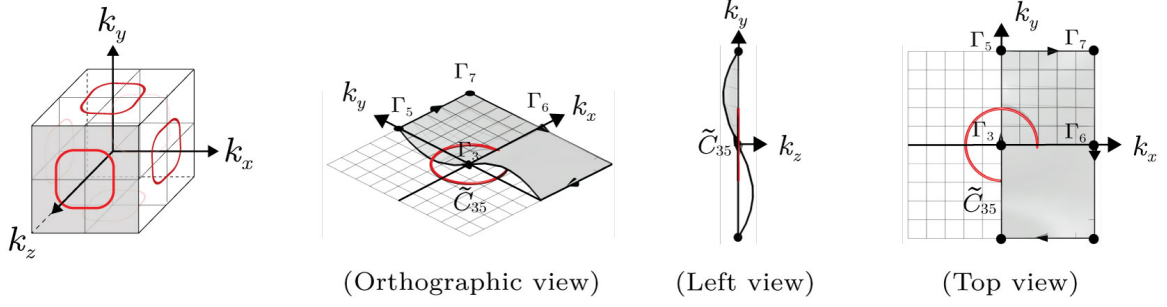


FIG. S4. Invariant loop avoiding intersection with the DLN. The loop c_{35} connecting Γ_3 and Γ_5 is bent down in the $-k_z$ direction, while its time-reversed partner \tilde{c}_{35} is bent up in the k_z direction. The corresponding interior surface S_{3567} is threaded once by the DLN (illustrated by a red circle).

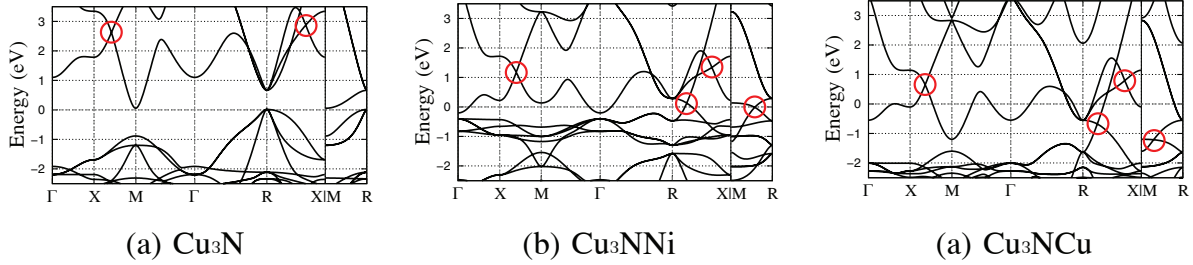


FIG. S5. Band structures of Cu_3NX , with $X=\{\text{V}_0, \text{Ni}, \text{Zn}\}$. (a) Cu_3N . (b) Cu_3NNi , and (c) Cu_3NCu . The Dirac nodes are indicated by red circles.

doping concentration x ($x < 1$). For this purpose, we first present the band structures of Cu_3NX , with $X=\{\text{Ni}, \text{Cu}\}$ in Fig. S5. These bands structures, including those of Cu_3NZn and Cu_3NPd are more or less similar, when considering the position-shift of the Fermi energy due to the electron valence of the TM dopants. The Fermi energy positions one band higher in the group XII TM-doped case, comparing to that of the group X TM-doped cases, due to two more valence electrons in the group XII TMs than in the group X TMs. Comparing to the band structure of Cu_3N in Fig. S5(a), it is clear that the group XII TMs provide two electrons per unit cell of Cu_3N , and thus move the preexisting DLNs near the Fermi energy. This indicates that a high doping concentration x should be essential in the realization of the DLN near the Fermi energy in the group XII -doped systems.

However, in the group X -doped systems, such as Cu_3NPd , and Cu_3NNi [see Fig. S5(b)], these high concentrations ($x \sim 1$) are unnecessary. Under the doping of the group X TMs, the Fermi level remains in the same region as where it was in Cu_3N , and instead doping drives the band-inversion. Therefore, DLNs start to appear near the Fermi energy in a lower concentration regime. To demonstrate this, we calculate the band structures of Cu_3NPd_x , with $x = 0.0, 0.125, 0.25, 0.5, 0.75$ and 1.0 by varying the number of Pd atoms in a $2 \times 2 \times 2$ supercell of Cu_3N . The results, presented in Fig S6, show that the

conduction and valence bands are already inverted even at $x = 0.125$, and that the degree of the band inversion, as well as the size of the DLN, increase with increasing doping concentration x .

Lastly, we consider the spin-orbit interaction in Cu_3NPd . In Fig. S7, we present the band structures of Cu_3NPd calculated with and without spin-orbit coupling (SOC). It is clear that the SOC induces a sizable gap in the DLNs up to ~ 62 meV along the R - X high-symmetry line in the BZ. However, the SOC cannot completely gap out the entire DLN, as a single nodal point on the R - X line additionally protected by a C_4 rotational symmetry. The states forming the nodal point have distinct eigenvalues of the rotational symmetry operation, and thus retain the degeneracy even in the presence of the SOC. This is in fact one of the mechanisms which stabilizes three-dimensional Dirac (3D) semimetals [5, 38, 40]. Therefore one might expect the 3D Dirac semimetal phase to be present in Cu_3NPd . However, considering that the SOC mainly comes from the $4d$ orbitals of Pd, and that the calculated SOC gap is estimated based on a somewhat extreme condition that Pd atoms are fully doped (one per unitcell of Cu_3N), it is more likely that the DLN semimetal should persist in a wide range of the Pd-doping concentration, and should be especially robust in the low-concentration regime. In order to strengthen (weaken) the SOC, one can substi-

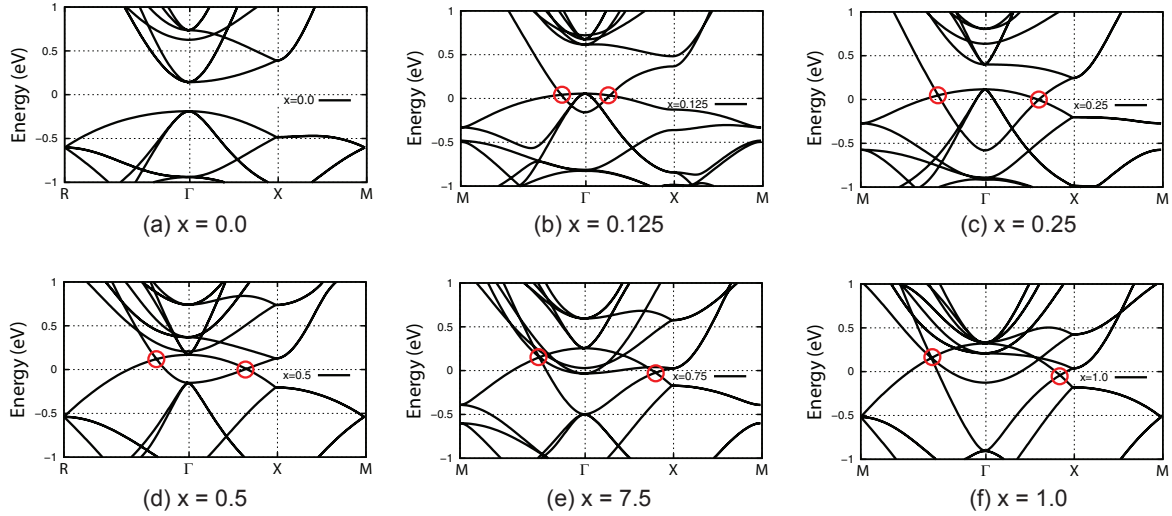


FIG. S6. Band structures of Cu_3NPd_x . (a) $x = 0.0$, (b) $x = 0.125$, (c) $x = 0.25$, (d) $x = 0.5$, (e) $x = 0.75$, (f) $x = 1.0$. The Dirac nodes are indicated by red circles.

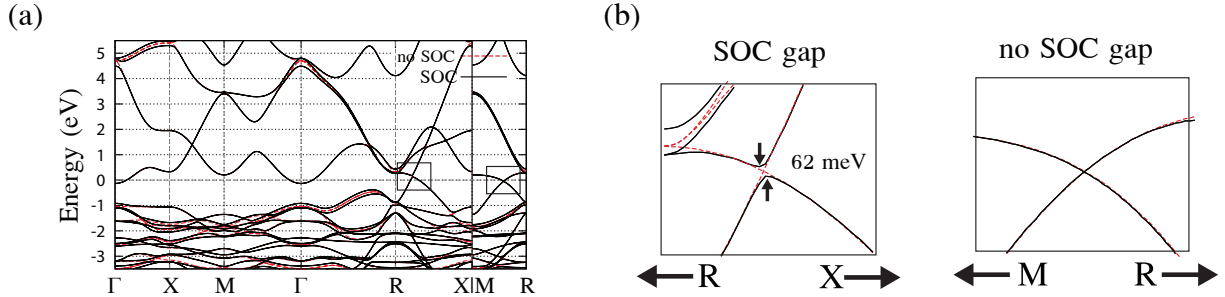


FIG. S7. Band structures of Cu_3NPd with and without spin-orbit interaction. The bands in the rectangles in (a) are magnified in (b).

tute the dopants from $4d$ TMs to $5d$ ($3d$) TMs such as Pt ($3d$ Ni). One can even dope with magnetic TMs to explore the effect of time-reversal-symmetry-breaking in the parent DLN semimetals.

-
- [1] M. Z. Hasan and C. L. Kane, Rev. Mod. Phys. **82**, 3045 (2010).
 - [2] X.-L. Qi and S.-C. Zhang, Rev. Mod. Phys. **83**, 1057 (2011).
 - [3] L. Fu, Phys. Rev. Lett. **106**, 106802 (2011).
 - [4] X. Wan, A. M. Turner, A. Vishwanath, and S. Y. Savrasov, Phys. Rev. B **83**, 205101 (2011).
 - [5] S. M. Young, S. Zaheer, J. C. Y. Teo, C. L. Kane, E. J. Mele, and A. M. Rappe, Phys. Rev. Lett. **108**, 140405 (2012).
 - [6] J. A. Steinberg, S. M. Young, S. Zaheer, C. L. Kane, E. J. Mele, and A. M. Rappe, Phys. Rev. Lett. **112**, 036403 (2014).

- [7] A. Alexandradinata, C. Fang, M. J. Gilbert, and B. A. Bernevig, Phys. Rev. Lett. **113**, 116403 (2014).
- [8] A. H. Castro Neto, F. Guinea, N. M. R. Peres, K. S. Novoselov, and A. K. Geim, Rev. Mod. Phys. **81**, 109 (2009).
- [9] H. Weng, Y. Liang, Q. Xu, Y. Rui, Z. Fang, X. Dai, and Y. Kawazoe, "Topological Node-Line Semimetal in Three Dimensional Graphene Networks," (2014), arXiv:1411.2175.
- [10] G. E. Volovik, "Flat band in topological matter: possible route to room-temperature superconductivity," (2011), arXiv:1110.4469.
- [11] H.-S. Kim, Y. Chen, and H.-Y. Kee, "Surface States of Perovskite Iridates AIrO_3 ; Signatures of Topological Crystalline Metal with Nontrivial \mathbb{Z}_2 Index," (2014), arXiv:1411.1406.
- [12] Y. Chen, Y.-M. Lu, and H.-Y. Kee, Nat. Commun. **6**, 6593 (2015).
- [13] H. Weng, C. Fang, Z. Fang, B. A. Bernevig, and X. Dai, Phys. Rev. X **5**, 011029 (2015).
- [14] Since $[\mathcal{H}(\mathbf{k}), \mathcal{PT}] = 0$, this \mathbb{Z}_2 invariant can also be understood as characterizing one parameter families of

- Hamiltonians in class AI [41].
- [15] L. Fu, C. L. Kane, and E. J. Mele, Phys. Rev. Lett. **98**, 106803 (2007).
 - [16] L. Fu and C. L. Kane, Phys. Rev. B **76**, 045302 (2007).
 - [17] R. Juza and H. Hahn, Zeitschrift für anorganische und allgemeine Chemie **239**, 282 (1938).
 - [18] F. Hadian, A. Rahmati, H. Movla, and M. Khaksar, Vacuum **86**, 1067 (2012).
 - [19] F. Gulo, A. Simon, J. Khler, and R. K. Kremer, Angewandte Chemie International Edition **43**, 2032 (2004).
 - [20] Z. Hou, Solid State Sciences **10**, 1651 (2008).
 - [21] M. G. Moreno-Armenta, W. L. Prez, and N. Takeuchi, Solid State Sciences **9**, 166 (2007).
 - [22] U. Zachwieja and H. Jacobs, Journal of the Less Common Metals **161**, 175 (1990).
 - [23] U. Hahn and W. Weber, Phys. Rev. B **53**, 12684 (1996).
 - [24] A. Ji, C. Li, and Z. Cao, Applied Physics Letters **89**, 252120 (2006).
 - [25] M. Sieberer, S. Khmelevskiy, and P. Mohn, Phys. Rev. B **74**, 014416 (2006).
 - [26] M. G. Moreno-Armenta, A. Martinez-Ruiz, and N. Takeuchi, Solid State Sciences **6**, 9 (2004).
 - [27] X. Fan, Z. Wu, G. Zhang, C. Li, B. Geng, H. Li, and P. Yan, Journal of Alloys and Compounds **440**, 254 (2007).
 - [28] J. Pierson and D. Horwat, Scripta Materialia **58**, 568 (2008).
 - [29] Z. Wu, H. Chen, N. Gao, E. Zhang, J. Yang, T. Yang, X. Li, and W. Huang, Computational Materials Science **95**, 221 (2014).
 - [30] X. Cui, A. Soon, A. Phillips, R. Zheng, Z. Liu, B. Delley, S. Ringer, and C. Stampfl, Journal of Magnetism and Magnetic Materials **324**, 3138 (2012).
 - [31] J. P. Perdew, K. Burke, and M. Ernzerhof, Phys. Rev. Lett. **77**, 3865 (1996).
 - [32] P. Giannozzi *et al.*, Journal of Physics: Condensed Matter **21**, 395502 (2009).
 - [33] A. M. Rappe, K. M. Rabe, E. Kaxiras, and J. D. Joannopoulos, Phys. Rev. B **41**, 1227 (1990).
 - [34] N. J. Ramer and A. M. Rappe, Phys. Rev. B **59**, 12471 (1999).
 - [35] I. Grinberg, N. J. Ramer, and A. M. Rappe, Phys. Rev. B **62**, 2311 (2000).
 - [36] See the supplementary material for the discussion on the doping concentration.
 - [37] R. Jackiw and C. Rebbi, Phys. Rev. D **13**, 3398 (1976).
 - [38] Z. Wang, H. Weng, Q. Wu, X. Dai, and Z. Fang, Phys. Rev. B **88**, 125427 (2013).
 - [39] L. S. Xie, L. M. Schoop, E. M. Seibel, Q. D. Gibson, W. Xie, and R. J. Cava, “Potential ring of Dirac nodes in a new polymorph of Ca_3P_2 ,” (2015), arXiv:1504.01731.
 - [40] Z. Wang, Y. Sun, X.-Q. Chen, C. Franchini, G. Xu, H. Weng, X. Dai, and Z. Fang, Phys. Rev. B **85**, 195320 (2012).
 - [41] J. C. Y. Teo and C. L. Kane, Phys. Rev. B **82**, 115120 (2010).